Spectroscopic factors in dripline nuclei

J. Wylie,[1,2] J. Okołowicz,[3] W. Nazarewicz,[4,2] M. Płoszajczak,[5]
S.M. Wang (王思敏),[6,7] X. Mao (毛兴泽),[1,2] and N. Michel[8,9]

[1]*National Superconducting Cyclotron Laboratory, Michigan State University, East Lansing, Michigan 48824, USA*
[2]*Department of Physics and Astronomy, Michigan State University, East Lansing, Michigan 48824, USA*
[3]*Institute of Nuclear Physics, Polish Academy of Sciences, Radzikowskiego 152, PL-31342 Kraków, Poland*
[4]*Facility for Rare Isotope Beams, Michigan State University, East Lansing, Michigan 48824, USA*
[5]*Grand Accélérateur National d'Ions Lourds (GANIL), CEA/DSM - CNRS/IN2P3, BP 55027, F-14076 Caen Cedex, France*
[6]*FRIB/NSCL Laboratory, Michigan State University, East Lansing, Michigan 48824, USA*
[7]*Institute of Modern Physics, Fudan University, Shanghai 200433, China*
[8]*Institute of Modern Physics, Chinese Academy of Sciences, Lanzhou 730000, China*
[9]*School of Nuclear Science and Technology, University of Chinese Academy of Sciences, Beijing 100049, China*

(Dated: July 16, 2021)

Single-nucleon knockout reaction studies of the proton-dripline nuclei ^{9}C and ^{13}O suggest an appreciable suppression of spectroscopic factors. In this work, we calculate the one-neutron and one-proton spectroscopic factors for the mirror pair ^{9}C-^{9}Li and ^{13}O using two variants of the continuum shell model: the complex-energy Gamow Shell Model and the real-energy Shell Model Embedded in the Continuum. Our results indicate that the continuum effects strongly suppress the spectroscopic factors of well-bound orbits in the dripline systems, but have less impact on the spectroscopic factors of weakly-bound states.

Introduction.—Spectroscopic factors (SFs) extracted from $(e, e'p)$ experiments yield the ∼35% quenching with respect to the shell model values [1]. Several mechanisms have been put forward to explain this reduction. These include the effects of short-range and long-range correlations [2–4]. In a series of papers [5–7], it was found that the ratio $R_s = \sigma_{\rm exp}/\sigma_{\rm th}$ of the experimental and theoretical inclusive one-nucleon removal cross section for a large number of projectiles shows a strong dependence on the $\Delta S = S_p - S_n$ asymmetry of the neutron and proton separation energies. Numerous papers have discussed the isospin dependence of SFs [8–14], or lack of it [15–17], see the recent review [4] for a comprehensive discussion and additional references.

However, the problem remains open both experimentally and theoretically. Experimental studies of $(p, 2p)$ reactions on oxygen and carbon isotopes did not find a significant dependence of SFs on proton-neutron asymmetry [15, 18]. A similar conclusion has been made in theoretical studies of neon isotopes and mirror nuclei ^{24}Si, ^{24}Ne and ^{28}S, ^{28}Mg [19]. On the other hand, coupled-cluster studies [20] of the neutron-rich oxygen isotopes have shown a significant quenching of SFs due to enhanced many-body correlations induced by a coupling to the scattering continuum above the neutron emission thresholds. As concluded in [7], the physical origins of the presented systematic behavior of R_s versus ΔS remains unresolved.

Based on the dispersive optical model analysis of proton scattering data [21, 22], one might hypothesise that the essential ingredient behind the systematics of R_s is the dispersion relation which connects real and imaginary parts of the scattering matrix. Following this line of reasoning, one can argue that the understanding of the $R_s(\Delta S)$ systematics should be related to the theoretical treatment of the nuclear openness, i.e., to a treatment of the coupling between bound states and the non-resonant (scattering) continuum.

The objective of this Letter to investigate the role of the continuum coupling on SFs in weakly-bound/unbound nuclei. To this end, by means of open-quantum-system configuration-interaction frameworks, we study one-proton and one-neutron removal SFs from proton-rich ^{9}C, ^{9}Li, ^{13}O, and ^{13}F, and neutron-rich ^{9}Li. This choice has been driven by the recent experimental studies [23, 24].

Method.—To provide a comprehensive description of continuum coupling effects, in this Letter, we adopt two different open-quantum-system frameworks: the Gamow Shell Model (GSM) [25, 26] and the Shell Model Embedded in the Continuum (SMEC) [27, 28], which have been successfully used for studies of weakly bound and unbound states in dripline nuclei. Both frameworks describe the nucleus as a core surrounded by valence nucleons, and treat the coupling to the unbound continuum space differently. In the GSM, the continuum effects are automatically taken into account by utilizing the Berggren ensemble [29] that contains resonant (bound and decaying) and scattering states. In the SMEC, based on the Feshbach projection technique, the continuum space consist of one nucleon occupying scattering states. By comparing the calculated SFs with the results obtained by the standard closed-quantum-system (CQS) shell model, the continuum effects on SFs can be quantified.

The Hermitian GSM Hamiltonian can be written as a sum of the kinetic energy of valence nucleons, the one-body core-valence interaction $U_{\rm c}(i)$, the two-body interaction $V_{i,j}$, and the two-body recoil term, where $i, j = 1, \ldots N_v$ and N_v is the number of valence nucle-

ons. The recoil term $\propto \sum \boldsymbol{p}_i \boldsymbol{p}_j$ [30] is used to restore the translational invariance. The GSM Hamiltonian is diagonalized in the Berggren basis $|k_p\rangle$. In this way, the continuum couplings between Slater determinants involving bound and unbound nucleons are automatically taken into account.

In a multi-channel version of SMEC, which is used here, the Hilbert space is divided into two orthogonal subspaces $\mathcal{Q}_0$ and $\mathcal{Q}_1$ containing 0 and 1 particle in the scattering continuum, respectively. The energy-dependent effective Hamiltonian of SMEC $\mathcal{H}(E)$ can be decomposed into the CQS shell-model (SM) Hamiltonian $H_{\mathcal{Q}_0\mathcal{Q}_0}$ acting in $\mathcal{Q}_0$ and the continuum coupling term $W_{\mathcal{Q}_0\mathcal{Q}_0}(E) = H_{\mathcal{Q}_0\mathcal{Q}_1} G^{(+)}_{\mathcal{Q}_1}(E) H_{\mathcal{Q}_1\mathcal{Q}_0}$, where $G^{(+)}_{\mathcal{Q}_1}$ is the one-nucleon Green's function and $H_{\mathcal{Q}_0\mathcal{Q}_1}$ and $H_{\mathcal{Q}_1\mathcal{Q}_0}$ are the coupling terms between subspaces $\mathcal{Q}_0$ and $\mathcal{Q}_1$. The mixing of SM eigenstates due to the continuum coupling interaction consists of the Hermitian principal value integral describing virtual continuum excitations and the anti-Hermitian residuum that represents the irreversible decay out of the internal space $\mathcal{Q}_0$.

Spectroscopic factors.— While not observables in the strictest sense [31–34], SFs are useful as they capture information on configuration mixing in the many-body wave function. In GSM, SFs are defined in terms of spectroscopic amplitudes $\mathcal{A}_{\ell j}(k_p) = \langle \Psi_A || a^+_{\ell j}(k_p) || \Psi_{A-1} \rangle / \sqrt{2J_A+1}$:

$$\mathcal{S}^2_{\ell j} = \sum\!\!\!\!\!\!\int \mathcal{A}^2_{\ell j}(k_p), \tag{1}$$

where Ψ_A is the wave function of the mass-A system, J_A is its total angular momentum, and $a^+_{\ell j}(k_p)$ is a nucleon creation operator associated with the Berggren basis state $|k_p\rangle$. It is to be noted that Eq. (1) involves the summation over discrete resonant states and integration along the contour of scattering states of the Berggren ensemble. In this way, $\mathcal{S}^2_{\ell j}$ is independent on the choice of the single-particle basis [35]. In the GSM framework, the complex conjugation arising in the dual space affects only the angular part and leaves the radial part unchanged, and this affects the definition of the scalar product in (1).

Due to the coupling to one-nucleon decay channel(s), the SMEC eigenfunction $\Psi_{A,\alpha}$ is a linear combination of SM wave functions $\Phi_{A,i}$: $\Psi_{A,\alpha} = \sum_i b_{A,\alpha i} \Phi_{A,i}$. In the standard version of SMEC, dubbed SMEC1, the spectroscopic amplitude between SMEC state $\Psi_{\alpha,A}$ and the SM state Φ^i_{A-1} becomes: $\mathcal{A}^{i\alpha}_{\ell_j} = \sum_k \mathcal{A}^{ik}_{\ell_j} b_{A,\alpha k}$. By including the continuum coupling in the $A-1$ nucleus, one obtains: $\mathcal{A}^{\beta\alpha}_{\ell_j} = \sum_{i,k} b_{A-1,\beta i} \mathcal{A}^{ik}_{\ell_j} b_{A,\alpha k}$. This version of calculations is referred to SMEC2. The spectroscopic factor in SMEC is defined as the sum of squared spectroscopic amplitudes associated with possible reaction channels. For instance, for the proton knockout $^{13}\mathrm{O}(3/2^-_{\mathrm{g.s.}}) \rightarrow {}^{12}\mathrm{N}(1^+_{\mathrm{g.s.}})$, both $p_{3/2}$ and $p_{1/2}$ partial waves contribute and their SFs are added.

Model space and parameters.—For the core, we took the tightly bound ^{4}He nucleus. The GSM Hamiltonian was defined as in Ref. [36, 37]. Namely, the core-nucleus potential $U_{\mathrm{c}}(i)$ was taken in the Woods-Saxon (WS) form (supplemented by a spin-orbit term and Coulomb potential), and a Furutani-Horiuchi-Tamagaki (FHT) force [38] was used to describe the two-body interaction $V_{i,j}$. The parameters for the potentials were taken from Ref. [37] for the *ps*-shell model space. For comparison, *p*-shell SM calculations in the harmonic oscillator basis (HO-SM) were carried out with the same GSM Hamiltonian. The single-particle (s.p.) energies in the HO-SM approximation were given by real parts of resonant states generating the GSM basis. In order to reveal the impact of higher-ℓ shells, we extended the model space to the *psd*-shell. In this case, the core potential strength for protons was readjusted until the ground-state (g.s.) energy of ^{8}C was within 0.2 MeV of the experimental value [39]. Once the model parameters were determined for ^{8}C, they were used for neutrons in the calculations for the mirror partners of ^{8,9}C (^{8}He,^{9}Li). The adjusted proton WS parameters were retained for ^{8}B,^{9}C, and the neutron parameters were taken from Ref. [37]. The same procedure was used to calculate the mirror pair (^{8,9}Li). Due to the fact that ^{9}C is particle-bound, the $A = 9$ nuclei were calculated with only two particles allowed in the continuum space (N_{cont}=2) as compared to N_{cont}=4 for $A = 8$. The complex-momentum contour defining the scattering part of the Berggren basis was divided into 3 segments: $[0, k_{\mathrm{peak}}]$, $[k_{\mathrm{peak}}, k_{\mathrm{mid}}]$, and $[k_{\mathrm{mid}}, k_{\mathrm{max}}]$, with the values $k_{\mathrm{peak}} = 0.3\,\mathrm{fm}^{-1}$, $k_{\mathrm{mid}} = 0.4\,\mathrm{fm}^{-1}$, and the cutoff momentum $k_{\mathrm{max}} = 4\,\mathrm{fm}^{-1}$. Each segment was discretized with 5 Gaussian points. The binding energies and spectra of $A = 8$,9 dripline nuclei obtained in our GSM calculations are discussed in the supplemental material [40]. The energy levels of mirror nuclei are reproduced fairly well, which suggest that the Coulomb energy displacement and the Thomas-Ehrman shift are under control in the GSM model.

In the SMEC calculations, the SM Hamiltonian $H_{\mathcal{Q}_0\mathcal{Q}_0}$ was taken as the standard YSOX interaction [41] in the $4\hbar\omega$ (*psd*)-model space. The radial s.p. wave functions (in Q_0) and the scattering wave functions (in Q_1) are generated by the WS central potential supplemented by the spin-orbit and Coulomb terms with the parameters of Ref. [42]. The continuum-coupling term $W_{\mathcal{Q}_0\mathcal{Q}_0}$ has been modeled by the Wigner-Bartlett contact interaction [42] described by two physically relevant parameters: the overall continuum-coupling strength V_0 and the spin-exchange parameter α that can be used to study the isospin content of the continuum coupling. Physically reasonable values of $|V_0|$ are in the interval 100-350 MeV·fm^3. As discussed in the earlier papers [43–45] the value $\alpha = 2$ is appropriate for dripline nuclei, and we adopted this value in this Letter.

To gain insights into the wave function fragmentation caused by the continuum coupling, we shall study two situations: (i) knockout of well-bound, minority species, nucleons, i.e., neutrons (protons) from proton-(neutron-) rich nuclei and (ii) knockout of weakly-bound, majority

species, nucleons, i.e., protons (neutrons) from proton-(neutron-)rich nuclei. For earlier studies of this problem, see coupled-cluster calculations in the Berggren basis [20] and the intranuclear-cascade model involving core excitations [46].

Knockout of well-bound nucleons.— We first study the removal of the $p_{3/2}$ neutron from the $J^\pi = 3/2^-$ g.s. of ^{9}C. Since the neutron separation energy in ^{9}C is large, the neutron is removed from a well-bound orbit. Table I shows the SFs calculated in GSM with different numbers of particles allowed to occupy scattering states. The GSM results are compared with the HO-SM calculations, in which the continuum effect is absent. In HO-SM, a SF of 0.86 is obtained, while this value becomes 0.67 in the GSM calculations when considering continuum coupling from the *ps*-shell. The inclusion of the *d*-shell leads to a further reduction of the SF down to $\mathcal{S}^2 = 0.48$ when four protons are allowed to occupy scattering states. A significant reduction of the SF with respect to the HO-SM value is also predicted for the removal of the well-bound $p_{3/2}$ proton from the g.s. of ^{9}Li.

TABLE I. Spectroscopic factors for the knockout of a $p_{3/2}$ nucleon from the $3/2^-$ g.s. of ^{9}C and ^{9}Li to the g.s. of ^{8}C, ^{8}He, ^{8}B, and ^{8}Li. The experimental neutron and proton separation energies [39] are shown (in MeV). The GSM-*ps* results were obtained in the full *ps* space while the GSM-*psd* space additionally includes scattering *d*-waves. The HO-SM result corresponds to the shell model calculation in the $0p$ space. $N_{\rm cont}$ is the number of particles allowed in non-resonant continuum of $A = 8$ nuclei.

Model	$N_{\rm cont}$	^{9}C→^{8}C	^{9}Li→^{8}He	^{9}C→^{8}B	^{9}Li→^{8}Li
		14.22	13.94	1.30	4.06
HO-SM	0	0.86	0.85	0.95	0.96
GSM-*ps*	3	0.67	0.67	0.98	0.98
GSM-*psd*	3	0.60	0.67	0.89	0.88
GSM-*psd*	4	0.48	0.65	0.89	0.88

The results shown in Table I indicate that the continuum couplings significantly reduce the SF for the knockout of well-bound nucleons from dripline nuclei. In order to understand the underlying mechanism, the squared spectroscopic amplitudes $\mathcal{A}^2_{p_{3/2}}(k_p)$ of the non-resonant states contributing to the spectroscopic factor $\mathcal{S}^2_{p_{3/2}}$ for the knockout of minority species nucleons from ^{9}C and ^{9}Li are shown in Fig. 1(a) and Fig. 1(c), respectively. Since the orbital $0p_{3/2}$ is well bound, the $p_{3/2}$ continuum is not expected to contribute. Indeed the value of the SF is determined by the contribution from the $0p_{3/2}$ bound pole, which is, however, significantly reduced compared to the HO-SM prediction, see Table. I

To understand this reduction, Fig. 2 compares the HO-SM wave-function decomposition to that of GSM-*psd* ($N_{\rm cont}$=4) for the six nuclei considered. It is seen that the continuum plays different roles in ^{8}C and ^{9}C. For the unbound ^{8}C, there is a broad distribution of GSM configurations involving non-resonant states, which are absent

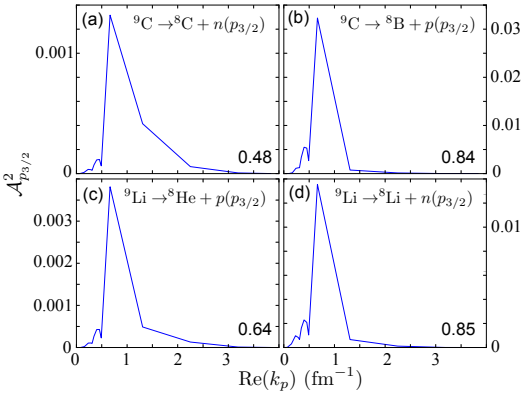

FIG. 1. Non-resonant contributions $\mathcal{A}^2_{p_{3/2}}(k_p)$ to the spectroscopic factor $\mathcal{S}^2_{p_{3/2}}$ for the knockout of nucleons from ^{9}C (top) and ^{9}Li (bottom) calculated in the GSM-*psd* space with $N_{\rm cont} = 4$. The numbers mark the squared spectroscopic amplitude of the $0p_{3/2}$ resonant state. The non-resonant contributions are multiplied by the integration weights as the contour integral in (1) has been discretized.

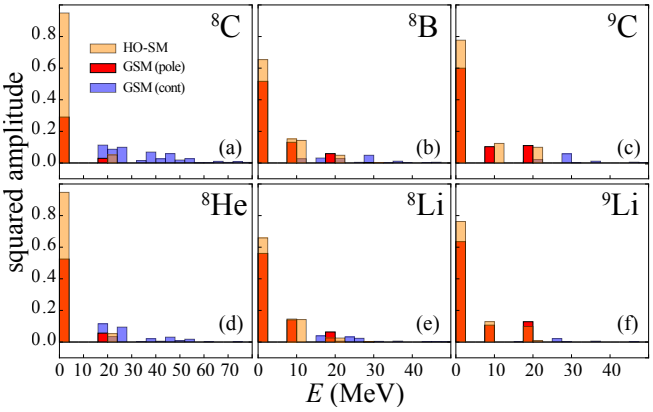

FIG. 2. Squared HO-SM and GSM amplitudes of shell-model configurations for ^{8}C (a), ^{8}B (b), ^{9}C (c), ^{8}He (d), ^{8}Li (e), and ^{9}Li (f). GSM calculations were performed in *psd* space with $N_{\rm cont}$=4. The contributions from the GSM pole space and scattering continuum space is shown separately. The configuration energy is defined as the sum of s.p. energies of valence nucleons relative to the SM configuration with the lowest energy. Note that the GSM amplitudes are generally complex, hence only their real parts are shown.

in the HO-SM calculations. For the particle-bound ^{9}C, the impact of the continuum on the dominant HO-SM configurations is not as dramatic.

The GSM weights of dominant configurations in the proton-unbound ^{8}C are: 29% for $\pi(0p_{3/2})^4$, 30% for $\pi(0p_{3/2})^3(p^{\rm cont}_{3/2})$, and 21% for $\pi(0p_{3/2})^2(p^{\rm cont}_{3/2})^2$. For ^{9}C, the leading configurations are: $\pi(0p_{3/2})^4\nu(0p_{3/2})$ (60%), $\pi(0p_{3/2})^3(p^{\rm cont}_{1/2})\nu(0p_{3/2})$ (10%), and $\pi(0p_{3/2})^2(0p_{1/2})^2\nu(0p_{1/2})$ (9%). It is seen, therefore, that the structure of ^{8}C differs significantly from the proton structure of ^{9}C. This results in a dra-

matic reduction of the $\nu 0p_{3/2}$ bound pole contribution and the quenching of the SF seen in Table I. A similar situation is predicted for the ^{9}Li→^{8}He+p process. As seen in Fig. 2, the structures of the mirror nuclei ^{9}Li and ^{9}C are very similar. In ^{8}He, the contribution from the pole space is larger than in ^{8}C as this nucleus is neutron-bound. Hence the reduction of the corresponding SF is less dramatic.

To further illustrate the quenching of neutron spectroscopic factors in proton-dripline nuclei, in Fig. 3(a) we show SMEC results for the one-neutron knockout from the g.s. of ^{13}O to the unbound g.s. of ^{12}O, which can decay by the emission of two protons [23]. The calculations have been carried out by assuming the resonant character of the ground state of ^{12}O (SMEC2) and by ignoring the unbound nature of this nucleus (SMEC1). One can see that opening of the proton emission channel in SMEC2 leads to a dramatic decrease of the neutron SF. This is consistent with the GSM results for ^{9}C.

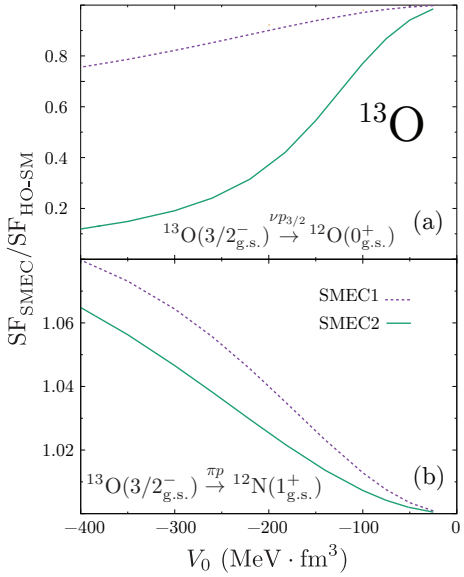

FIG. 3. The ratio of spectroscopic factors obtained in SMEC (SMEC1 and SMEC2 variants) and HO-SM for (a) neutron and (b) proton removal from the g.s. of ^{13}O as a function of the continuum-coupling strength V_0.

Removal of weakly-bound/unbound nucleons from dripline systems.— We begin from the GSM analysis of SFs for the removal of a majority species nucleon from ^{9}C and ^{9}Li. As seen in Table I, contrary to the removal of minority species nucleons, the SFs for ^{9}C(3/2$^-_{\rm g.s.}$) → $\pi p_{3/2}+{}^{8}$B(2$^+_{\rm g.s.}$) and ^{9}Li(3/2$^-_{\rm g.s.}$) → $\nu p_{3/2}+{}^{8}$Li(2$^+_{\rm g.s.}$) are weakly impacted by the continuum coupling, in spite of the fact that the contribution to the SFs from the scattering $p_{3/2}$ space increases, see Fig. 1(b,d). This behavior is due to the small separation energy, as the wave functions of valence nucleons have a broad spatial distribution. As a result, the mother nucleus can be viewed in terms of a weak coupling of the valence nucleon to a daughter nucleus core, which means that the nucleon-removal process has little impact on the core [7, 47]. This spectator approximation is nicely seen in the wave function amplitudes of mother and daughter nuclei in Fig. 2.

The large SFs for the removal of weakly bound/unbound nucleons are also seen in the SMEC calculation. Figure 3(b) illustrates the SF of ^{13}O(3/2$^-_{\rm g.s.}$) → ^{12}N(1$^+_{g.s.}$) $\ell = 1$ proton decay. Here, the removal of a proton yields the weakly bound ($S_p = 0.6$ MeV) g.s. of ^{12}N. Interestingly, the SF slightly increases with increasing the continuum-coupling strength. This is opposite to what was found for the neutron SFs (see Fig. 3(a)) but is consistent with the GSM results. The small difference between 'SMEC1' and 'SMEC2' results signifies that including the coupling to the closed channels has no significant effect on one-nucleon SFs.

A proton decay of a resonance in ^{13}F with a width $\Gamma = 1.01(27)$ MeV constitutes another excellent example of a large SF associated with a removal of an unbound nucleon from a dripline system . The exotic ^{13}F nucleus, recently observed in Ref. [24], is located four neutrons beyond the proton drip line. The resonance in question, placed 0.48(19) MeV above the proton decay threshold of ^{12}O(2$^+_2$), was preliminary identified as the 5/2$^+_1$ excited state. Due to the unbound character of ^{13}F, the SF of the 5/2$^+_1$ resonance has been calculated using SMEC2. The continuum coupling strength $V_0 = -100$ MeV·fm^3 reproduces the measured decay width. As one can see in Fig. 4, the ratio of SFs calculated in SMEC and HO-SM is large; its maximum appears close to the suggested experimental energy of the 5/2$^+_1$ resonance with respect to the one-proton decay threshold [^{12}O(2$^+_2$)⊗π] [24]. As we discussed above, this enhanced SF means that the wave function of the daughter nucleus is weakly coupled to the valence proton. This is not surprising as the decaying resonance lies very close to the threshold; hence, its wave function is threshold-aligned due to the continuum coupling [42].

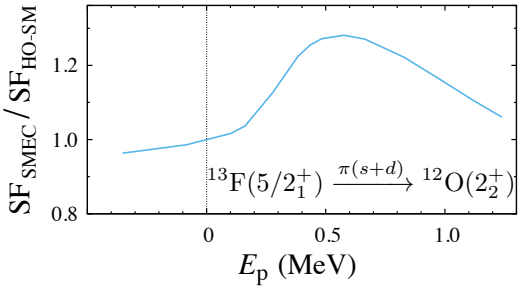

FIG. 4. Ratio between SFs obtained in SMEC2 and HO-SM for the 5/2$^+_1$ proton resonance in ^{13}F as a function of one-proton decay energy. Two partial proton waves, $s_{1/2}$ and $d_{5/2}$, primarily contribute to the SF. The dotted line at $E_p = 0$ MeV denotes the proton decay threshold [^{12}O(2$^+_2$)⊗π].

Summary.— Using two different formulations of the shell model for open quantum systems, we have demonstrated and explained a non-intuitive result that the

continuum-coupling effect on SFs is large for the removal process of a well-bound nucleon but is weak when the removed particle is weakly bound/unbound. This behavior can be naturally explained within the continuum SM in terms of coupling to the non-resonant space. *When a minority species nucleon is removed*, the daughter nucleus moves in the direction of the dripline. This leads to an appreciable change in configurations of weakly-bound nucleons that are impacted by continuum effects. For instance, in the cases considered, the daughter nuclei ^{8}C and ^{12}O are proton-unbound, and ^{8}He is a $4n$ halo. Consequently, the SF is reduced. *When a majority species nucleon is removed*, the daughter nucleus moves away from the dripline and stays closer to the core of the parent system. Consequently, based on the spectator approximation, one expects the SF to be large. This simple analysis demonstrates that to understand the generic behavior of the spectroscopic factors in dripline nuclei no short-range correlations need to be invoked.

The continuum couplings for nucleons in weakly-bound orbits depend on the number of particle continua (in GSM), the resonance nature of states involved, or (in SMEC) on the number of decay channels included and the value of the continuum coupling strength. Moreover, as shown in SMEC, the difference between the spectroscopic factor calculated in SMEC and in SM depends on the isospin structure of the interaction: for large $|S_n - S_p|$ the asymmetry appears between the nucleon-nucleon interaction in weakly-bound and well-bound systems and the interaction between unlike nucleons becomes reduced [48]. The effect depends on the angular momentum involved. For large $\ell > 3$, the asymmetry in a removal of minority/majority nucleon is expected to be reduced. Future theoretical studies should answer which of these two ingredients (continuum coupling or interaction effects) prevail in different mass regions of the periodic table.

Acknowledgements.— Discussions with Bob Charity and Lee Sobotka are gratefully acknowledged. This material is based upon work supported by the U.S. Department of Energy, Office of Science, Office of Nuclear Physics under Awards No.DE-SC0013365 (Michigan State University), No.DE-SC0018083 (NUCLEI SciDAC-4 collaboration), by the National Natural Science Foundation of China, the Chinese Academy of Sciences and Peking University under grants No.NPT2020KFY13 (the State Key Laboratory of Nuclear Physics and Technology, Peking University), No.11975282 (the National Natural Science Foundation of China), No. XDB34000000 (the Strategic Priority Research Program of Chinese Academy of Sciences), No.XDPB15 (the Key Research Program of the Chinese Academy of Sciences) and by the COPIN and COPIGAL French-Polish scientific exchange programs.

[1] L. Lapikás, "Quasi-elastic electron scattering off nuclei," Nucl. Phys. A **553**, 297–308 (1993).
[2] W. H. Dickhoff, "Determining and calculating spectroscopic factors from stable nuclei to the drip lines," J. Phys. G **37**, 064007 (2010).
[3] S. Paschalis, M. Petri, A. Macchiavelli, O. Hen, and E. Piasetzky, "Nucleon-nucleon correlations and the single-particle strength in atomic nuclei," Phys. Lett. B **800**, 135110 (2020).
[4] T. Aumann, C. Barbieri, D. Bazin, C. Bertulani, A. Bonaccorso, W. Dickhoff, A. Gade, M. Gómez-Ramos, B. Kay, A. Moro, T. Nakamura, A. Obertelli, K. Ogata, S. Paschalis, and T. Uesaka, "Quenching of single-particle strength from direct reactions with stable and rare-isotope beams," Prog. Part. Nucl. Phys. **118**, 103847 (2021).
[5] A. Gade et al., "Reduced occupancy of the deeply bound $0d_{5/2}$ neutron state in ^{32}Ar," Phys. Rev. Lett. **93**, 042501 (2004).
[6] A. Gade et al., "Reduction of spectroscopic strength: Weakly-bound and strongly-bound single-particle states studied using one-nucleon knockout reactions," Phys. Rev. C **77**, 044306 (2008).
[7] J. A. Tostevin and A. Gade, "Updated systematics of intermediate-energy single-nucleon removal cross sections," Phys. Rev. C **103**, 054610 (2021).
[8] C. Barbieri and W. H. Dickhoff, "Spectroscopic factors in ^{16}O and nucleon asymmetry," Int. J. Mod. Phys. A **24**, 2060–2068 (2009).
[9] F. Flavigny, A. Obertelli, A. Bonaccorso, G. F. Grinyer, C. Louchart, L. Nalpas, and A. Signoracci, "Nonsudden limits of heavy-ion induced knockout reactions," Phys. Rev. Lett. **108**, 252501 (2012).
[10] B. P. Kay, J. P. Schiffer, and S. J. Freeman, "Quenching of cross sections in nucleon transfer reactions," Phys. Rev. Lett. **111**, 042502 (2013).
[11] N. K. Timofeyuk, "Spectroscopic factors and asymptotic normalization coefficients for $0p$-shell nuclei: Recent updates," Phys. Rev. C **88**, 044315 (2013).
[12] J. A. Tostevin and A. Gade, "Systematics of intermediate-energy single-nucleon removal cross sections," Phys. Rev. C **90**, 057602 (2014).
[13] J. Lee et al., "Asymmetry dependence of reduction factors from single-nucleon knockout of ^{30}Ne at ∼230 MeV/nucleon," Prog. Theor. Exp. Phys. **2016** (2016), 10.1093/ptep/ptw096.
[14] S. T. Wang, Y. P. Xu, and D. Y. Pang, "Energy dependence of the reduced single-particle strength for strongly-bound proton removal on ^{16}C," Phys. Scr. **94**, 015302 (2018).
[15] L. Atar et al., "Quasifree (p, $2p$) reactions on oxygen isotopes: Observation of isospin independence of the reduced single-particle strength," Phys. Rev. Lett. **120**, 052501 (2018).
[16] M. Gómez-Ramos and A. Moro, "Binding-energy independence of reduced spectroscopic strengths derived from (p,2p) and (p,pn) reactions with nitrogen and oxygen isotopes," Phys. Lett. B **785**, 511 – 516 (2018).
[17] N. T. T. Phuc, K. Yoshida, and K. Ogata, "Toward a reliable description of (p, pn) reactions in the distorted-

wave impulse approximation," Phys. Rev. C **100**, 064604 (2019).
[18] M. Holl et al., "Quasi-free neutron and proton knockout reactions from light nuclei in a wide neutron-to-proton asymmetry range," Phys. Lett. B **795**, 682 – 688 (2019).
[19] J. Okołowicz, Y. Lam, M. Płoszajczak, A. Macchiavelli, and N. Smirnova, "Consistent analysis of one-nucleon spectroscopic factors involving weakly- and strongly-bound nucleons," Phys. Lett. B **757**, 303–306 (2016).
[20] O. Jensen, G. Hagen, M. Hjorth-Jensen, B. A. Brown, and A. Gade, "Quenching of spectroscopic factors for proton removal in oxygen isotopes," Phys. Rev. Lett. **107**, 032501 (2011).
[21] R. J. Charity, L. G. Sobotka, and W. H. Dickhoff, "Asymmetry dependence of proton correlations," Phys. Rev. Lett. **97**, 162503 (2006).
[22] R. J. Charity, J. M. Mueller, L. G. Sobotka, and W. H. Dickhoff, "Dispersive-optical-model analysis of the asymmetry dependence of correlations in ca isotopes," Phys. Rev. C **76**, 044314 (2007).
[23] R. J. Charity, L. G. Sobotka, and J. A. Tostevin, "Single-nucleon knockout cross sections for reactions producing resonance states at or beyond the drip line," Phys. Rev. C **102**, 044614 (2020).
[24] R. J. Charity et al., "Observation of the exotic isotope ^{13}F located four neutrons beyond the proton drip line," Phys. Rev. Lett. **126**, 132501 (2021).
[25] N. Michel, W. Nazarewicz, M. Płoszajczak, and K. Bennaceur, "Gamow shell model description of neutron-rich nuclei," Phys. Rev. Lett. **89**, 042502 (2002).
[26] N. Michel, W. Nazarewicz, M. Płoszajczak, and T. Vertse, "Shell model in the complex energy plane," J. Phys. G **36**, 013101 (2009).
[27] K. Bennaceur, F. Nowacki, J. Okołowicz, and M. Płoszajczak, "Analysis of the ^{16}O(p,γ)^{17}F capture reaction using the shell model embedded in the continuum," Nucl. Phys. A **671**, 203–232 (2000).
[28] J. Okołowicz, M. Płoszajczak, and I. Rotter, "Dynamics of quantum systems embedded in a continuum," Phys. Rep. **374**, 271 – 383 (2003).
[29] T. Berggren, "On the use of resonant states in eigenfunction expansions of scattering and reaction amplitudes," Nucl. Phys. A **109**, 265–287 (1968).
[30] Y. Suzuki and K. Ikeda, "Cluster-orbital shell model and its application to the he isotopes," Phys. Rev. C **38**, 410–413 (1988).
[31] R. J. Furnstahl and H. W. Hammer, "Are occupation numbers observables?" Phys. Lett. B **531**, 203 (2002).
[32] T. Duguet, H. Hergert, J. D. Holt, and V. Somà, "Nonobservable nature of the nuclear shell structure: Meaning, illustrations, and consequences," Phys. Rev. C **92**, 034313 (2015).
[33] M. Gómez-Ramos, A. Obertelli, and Y. L. Sun, "Breakup reactions and their ambiguities," Eur. Phys. J. A **57**, 148 (2021).
[34] A. J. Tropiano, S. K. Bogner, and R. J. Furnstahl, "Short-range correlation physics at low RG resolution," (2021), arXiv:2105.13936 [nucl-th].
[35] N. Michel, W. Nazarewicz, and M. Płoszajczak, "Threshold effects in multichannel coupling and spectroscopic factors in exotic nuclei," Phys. Rev. C **75**, 031301 (2007).
[36] Y. Jaganathen, R. M. I. Betan, N. Michel, W. Nazarewicz, and M. Płoszajczak, "Quantified gamow shell model interaction for *psd*-shell nuclei," Phys. Rev. C **96**, 054316 (2017).
[37] X. Mao, J. Rotureau, W. Nazarewicz, N. Michel, R. M. Id Betan, and Y. Jaganathen, "Gamow-shell-model description of Li isotopes and their mirror partners," Phys. Rev. C **102**, 024309 (2020).
[38] H. Furutani, H. Horiuchi, and R. Tamagaki, "Cluster-Model Study of the T=1 States in A=4 System: 3He+p Scattering," Prog. of Theor. Phys. **62**, 981–1002 (1979), https://academic.oup.com/ptp/article-pdf/62/4/981/5338838/62-4-981.pdf.
[39] `http://www.nndc.bnl.gov/ensdf` (2015).
[40] See Supplemental Material at [URL inserted by publisher] for more details on the binding energies and spectra of $A = 8, 9$ dripline nuclei obtained in our GSM calculations and the tables of dominant GSM configurations.
[41] C. Yuan, T. Suzuki, T. Otsuka, F. Xu, and N. Tsunoda, "Shell-model study of boron, carbon, nitrogen, and oxygen isotopes with a monopole-based universal interaction," Phys. Rev. C **85**, 064324 (2012).
[42] J. Okołowicz, M. Płoszajczak, and W. Nazarewicz, "Convenient location of a near-threshold proton-emitting resonance in ^{11}B," Phys. Rev. Lett. **124**, 042502 (2020).
[43] Y. Luo, J. Okołowicz, M. Płoszajczak, and N. Michel, "Shell model embedded in the continuum for binding systematics in neutron-rich isotopes of oxygen and fluor," arXiv:nucl-th/0211068 (2002).
[44] N. Michel, W. Nazarewicz, J. Okołowicz, M. Płoszajczak, and J. Rotureau, "Shell model description of nuclei far from stability," Acta Physica Polonica B **35**, 1249–1261 (2004).
[45] R. J. Charity et al., "Spin alignment following inelastic scattering of ^{17}Ne, lifetime of ^{16}F, and its constraint on the continuum coupling strength," Phys. Rev. C **97**, 054318 (2018).
[46] C. Louchart, A. Obertelli, A. Boudard, and F. Flavigny, "Nucleon removal from unstable nuclei investigated via intranuclear cascade," Phys. Rev. C **83**, 011601 (2011).
[47] C. Hebborn and P. Capel, "Halo effective field theory analysis of one-neutron knockout reactions of ^{11}Be and ^{15}C," (2021), arXiv:2105.04490 [nucl-th].
[48] N. Michel and M. Płoszajczak, Gamow Shell Model (Springer, 2021).

Supplemental Material for "Spectroscopic factors in dripline nuclei"

J. Wylie,[1,2] J. Okołowicz,[3] W. Nazarewicz,[4,2] M. Płoszajczak,[5]
S.M. Wang (王思敏),[6,7] X. Mao (毛兴泽),[1,2] and N. Michel[8,9]

[1] *National Superconducting Cyclotron Laboratory, Michigan State University, East Lansing, Michigan 48824, USA*
[2] *Department of Physics and Astronomy, Michigan State University, East Lansing, Michigan 48824, USA*
[3] *Institute of Nuclear Physics, Polish Academy of Sciences, Radzikowskiego 152, PL-31342 Kraków, Poland*
[4] *Facility for Rare Isotope Beams, Michigan State University, East Lansing, Michigan 48824, USA*
[5] *Grand Accélérateur National d'Ions Lourds (GANIL), CEA/DSM - CNRS/IN2P3, BP 55027, F-14076 Caen Cedex, France*
[6] *FRIB/NSCL Laboratory, Michigan State University, East Lansing, Michigan 48824, USA*
[7] *Institute of Modern Physics, Fudan University, Shanghai 200433, China*
[8] *Institute of Modern Physics, Chinese Academy of Sciences, Lanzhou 730000, China*
[9] *School of Nuclear Science and Technology, University of Chinese Academy of Sciences, Beijing 100049, China*

(Dated: July 16, 2021)

This supplemental material contains supplemental discussion of the binding energies and spectra of $A = 8,9$ dripline nuclei obtained in our GSM calculations and the tables of dominant GSM configurations.

S.I. Spectra of mirror threshold $A = 8,9$ nuclei

Figure S1 shows the binding energies and spectra of $A = 8,9$ dripline nuclei obtained in our GSM calculations. On the proton-rich side, ^{8}C is proton-unstable, ^{8}B is a proton halo ($S_p = 136\,\text{keV}$) [1, 2], and ^{9}C has $S_p = 1.3\,\text{MeV}$. The mirror neutron-rich nuclei ^{8}He/^{8,9}Li are all neutron-bound. Here, the extremely neutron-rich ^{8}He is a four-neutron halo. It is seen that the energy levels of mirror nuclei are reproduced fairly well, which suggest that the Coulomb energy displacement and the Thomas-Ehrman shift are under control in the GSM model.

[1] R. E. Warner, J. H. Kelley, P. Zecher, F. D. Becchetti, J. A. Brown, C. L. Carpenter, A. Galonsky, J. Kruse, A. Muthukrishnan, A. Nadasen, R. M. Ronningen, P. Schwandt, B. M. Sherrill, J. Wang, and J. S. Winfield, "Evidence for a proton halo in ^{8}B: Enhanced total reaction cross sections at 20 to 60 mev/nucleon," Phys. Rev. C **52**, R1166–R1170 (1995).

[2] G. Korolev, A. Dobrovolsky, A. Inglessi, G. Alkhazov, P. Egelhof, A. Estradé, I. Dillmann, F. Farinon, H. Geissel, S. Ilieva, Y. Ke, A. Khanzadeev, O. Kiselev, J. Kurcewicz, X. Le, Y. Litvinov, G. Petrov, A. Prochazka, C. Scheidenberger, L. Sergeev, H. Simon, M. Takechi, S. Tang, V. Volkov, A. Vorobyov, H. Weick, and V. Yatsoura, "Halo structure of ^{8}B determined from intermediate energy proton elastic scattering in inverse kinematics," Phys. Lett. B **780**, 200–204 (2018).

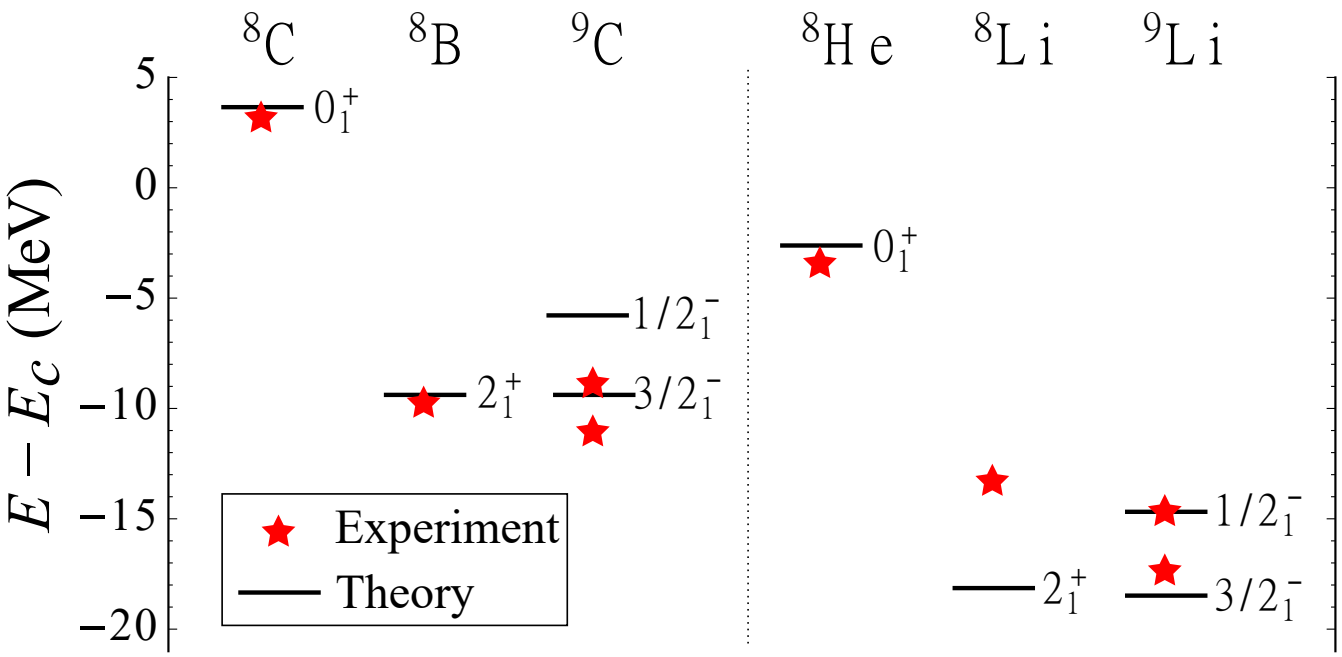

FIG. S1. GSM spectra of proton-rich nuclei ^{8,9}C and ^{8}B (left) and their neutron-rich mirror partners ^{8}He/^{8,9}Li (right) compared to experiment. Energies are shown with respect to the ^{4}He core.

S.II. Dominant GSM configurations

Tables S1-S4 show the dominant GSM configurations for each nucleus at *ps* and *psd* spaces. Only configurations with weights greater than 2% are listed.

TABLE S1. The dominant GSM configurations for ^{8}C and ^{9}C for two sets of GSM calculations. The first set of calculations was carried out in a *ps*-space with $N_{\rm cont} = 3$. The second set corresponds to *psd*-space and $N_{\rm cont} = 4$ in the continuum for ^{8}C. In both cases, only two particles were allowed in the continuum for ^{9}C.

Nucleus	J^π	$E^{\rm exp}(\Gamma^{\rm exp})$	$E^{\rm cal}(\Gamma^{\rm cal})$	Configuration
^{8}C$_{ps}$	0^+	3.483(0.23)	2.479(0.006)	45% $(0p_{3/2})^4$ 33% $(0p_{3/2})^3(p^{\rm scatt}_{3/2})$ 13% $(0p_{3/2})^2(p^{\rm scatt}_{3/2})^2$ 3% $(0p_{3/2})^2(0p_{1/2})^2$ 2% $(0p_{3/2})(p^{\rm scatt}_{1/2})^3$
^{9}C$_{ps}$	$3/2^-$	-10.742	-10.515	61% $(0p_{3/2})^4_{\rm p}(0p_{3/2})_{\rm n}$ 12% $(0p_{3/2})^3_{\rm p}(p^{\rm scatt}_{3/2})_{\rm p}(0p_{3/2})_{\rm n}$ 10% $(0p_{3/2})^3_{\rm p}(0p_{1/2})_{\rm p}(0p_{3/2})_{\rm n}$ 8% $(0p_{3/2})^2_{\rm p}(0p_{1/2})^2_{\rm p}(0p_{3/2})_{\rm n}$ 2% $(0p_{3/2})^2_{\rm p}(0p_{1/2})_{\rm p}(p^{\rm scatt}_{3/2})_{\rm p}(0p_{3/2})_{\rm n}$ 2% $(0p_{3/2})^2_{\rm p}(p^{\rm scatt}_{3/2})^2_{\rm p}(0p_{3/2})_{\rm n}$
	$1/2^-$	-8.56(0.1)	-7.583	60% $(0p_{3/2})^4_{\rm p}(0p_{3/2})_{\rm n}$ 17% $(0p_{3/2})^3_{\rm p}(0p_{1/2})_{\rm p}(0p_{3/2})_{\rm n}$ 9% $(0p_{3/2})^3_{\rm p}(p^{\rm scatt}_{3/2})_{\rm p}(0p_{1/2})_{\rm n}$ 4% $(0p_{3/2})^2_{\rm p}(0p_{1/2})^2_{\rm p}(0p_{1/2})_{\rm n}$ 3% $(0p_{3/2})^2_{\rm p}(0p_{1/2})_{\rm p}(p^{\rm scatt}_{3/2})_{\rm p}(0p_{3/2})_{\rm n}$ 2% $(0p_{3/2})^3_{\rm p}(p^{\rm scatt}_{3/2})_{\rm p}(0p_{3/2})_{\rm n}$
^{8}C$_{psd}$	0^+	3.483(0.23)	3.653(0.03)	29% $(0p_{3/2})^4$ 30% $(0p_{3/2})^3(p^{\rm scatt}_{3/2})$ 21% $(0p_{3/2})^2(p^{\rm scatt}_{3/2})^2$ 8% $(0p_{3/2})(p^{\rm scatt}_{3/2})^3$ 3% $(0p_{3/2})^2(0p_{1/2})^2$ 2% $(p^{\rm scatt}_{3/2})^4$
^{9}C$_{psd}$	$3/2^-$	-10.742	-9.385	60% $(0p_{3/2})^4_{\rm p}(0p_{3/2})_{\rm n}$ 10% $(0p_{3/2})^3_{\rm p}(0p_{1/2})_{\rm p}(0p_{3/2})_{\rm n}$ 9% $(0p_{3/2})^2_{\rm p}(0p_{1/2})^2_{\rm p}(0p_{1/2})_{\rm n}$ 9% $(0p_{3/2})^3_{\rm p}(p^{\rm scatt}_{3/2})_{\rm p}(0p_{3/2})_{\rm n}$ 2% $(0p_{3/2})^2_{\rm p}(p^{\rm scatt}_{3/2})^2_{\rm p}(0p_{3/2})_{\rm n}$ 2% $(0p_{3/2})^3_{\rm p}(0p_{1/2})_{\rm p}(0p_{1/2})_{\rm n}$
	$1/2^-$	-8.56(0.1)	-5.783	57% $(0p_{3/2})^4_{\rm p}(0p_{1/2})_{\rm n}$ 17% $(0p_{3/2})^3_{\rm p}(0p_{1/2})_{\rm p}(0p_{3/2})_{\rm n}$ 8% $(0p_{3/2})^3_{\rm p}(p^{\rm scatt}_{3/2})_{\rm p}(0p_{1/2})_{\rm n}$ 5% $(0p_{3/2})^2_{\rm p}(0p_{1/2})^2_{\rm p}(0p_{1/2})_{\rm n}$ 3% $(0p_{3/2})^2_{\rm p}(0p_{1/2})_{\rm p}(p^{\rm scatt}_{3/2})(0p_{3/2})_{\rm n}$ 2% $(0p_{3/2})^2_{\rm p}(p^{\rm scatt}_{3/2})^2_{\rm p}(0p_{1/2})_{\rm n}$ 2% $(0p_{3/2})^3_{\rm p}(p^{\rm scatt}_{3/2})_{\rm p}(0p_{3/2})_{\rm n}$

TABLE S2. Similar as in Table S1 but for ^{8}He and ^{9}Li. Only two particles were allowed in the continuum for ^{9}Li.

Nucleus	J^π	$E^{\rm exp}(\Gamma^{\rm exp})$	$E^{\rm cal}(\Gamma^{\rm cal})$	Configuration
^{8}He$_{ps}$	0^+	-3.112	-0.937	50% $(0p_{3/2})^4$ 31% $(0p_{3/2})^3(p^{\rm scatt}_{3/2})$ 11% $(0p_{3/2})^2(p^{\rm scatt}_{3/2})^2$ 4% $(0p_{3/2})^2(0p_{1/2})^2$ 2% $(0p_{3/2})(p^{\rm scatt}_{3/2})^3$
^{9}Li$_{ps}$	$3/2^-$	-17.045	-16.657	65% $(0p_{3/2})^4_{\rm n}(0p_{3/2})_{\rm p}$ 11% $(0p_{3/2})^3_{\rm n}(0p_{1/2})_{\rm n}(0p_{3/2})_{\rm p}$ 9% $(0p_{3/2})^2_{\rm n}(0p_{1/2})^2_{\rm n}(0p_{3/2})_{\rm p}$ 8% $(0p_{3/2})^3_{\rm n}(p^{\rm scatt}_{1/2})_{\rm n}(0p_{3/2})_{\rm p}$
	$1/2^-$	-14.354	-13.561	64% $(0p_{3/2})^4_{\rm n}(0p_{1/2})_{\rm p}$ 18% $(0p_{3/2})^3_{\rm n}(0p_{1/2})_{\rm n}(0p_{3/2})_{\rm p}$ 6% $(0p_{3/2})^3_{\rm n}(p^{\rm scatt}_{3/2})_{\rm n}(0p_{1/2})_{\rm p}$ 4% $(0p_{3/2})^2_{\rm n}(0p_{1/2})^2_{\rm n}(0p_{1/2})_{\rm p}$ 2% $(0p_{3/2})^2_{\rm n}(0p_{1/2})_{\rm n}(p^{\rm scatt}_{3/2})_{\rm n}(0p_{3/2})_{\rm p}$
^{8}He$_{psd}$	0^+	-3.112	-2.616	52% $(0p_{3/2})^4$ 25% $(0p_{3/2})^3(p^{\rm scatt}_{3/2})$ 10% $(0p_{3/2})^2(p^{\rm scatt}_{3/2})^2$ 6% $(0p_{3/2})^2(0p_{1/2})^2$ 2% $(0p_{3/2})(p^{\rm scatt}_{3/2})^3$
^{9}Li$_{psd}$	$3/2^-$	-17.045	-18.481	64% $(0p_{3/2})^4_{\rm n}(0p_{3/2})_{\rm p}$ 11% $(0p_{3/2})^2_{\rm n}(0p_{1/2})^2_{\rm n}(0p_{3/2})_{\rm p}$ 11% $(0p_{3/2})^3_{\rm n}(0p_{1/2})_{\rm n}(0p_{3/2})_{\rm p}$ 4% $(0p_{3/2})^3_{\rm n}(p^{\rm scatt}_{3/2})_{\rm n}(0p_{3/2})_{\rm p}$ 2% $(0p_{3/2})^3_{\rm n}(0p_{1/2})_{\rm n}(0p_{3/2})_{\rm p}$ 2% $(0p_{3/2})^2_{\rm n}(p^{\rm scatt}_{3/2})^2_{\rm n}(0p_{3/2})_{\rm p}$
	$1/2^-$	-14.354	-14.683	63% $(0p_{3/2})^4_{\rm n}(0p_{1/2})_{\rm p}$ 18% $(0p_{3/2})^3_{\rm n}(0p_{1/2})_{\rm n}(0p_{3/2})_{\rm p}$ 6% $(0p_{3/2})^2_{\rm n}(0p_{1/2})^2_{\rm n}(0p_{1/2})_{\rm p}$ 4% $(0p_{3/2})^3_{\rm n}(p^{\rm scatt}_{3/2})_{\rm n}(0p_{1/2})_{\rm p}$ 2% $(0p_{3/2})^2_{\rm n}(p^{\rm scatt}_{3/2})^2_{\rm n}(0p_{1/2})_{\rm p}$

TABLE S3. Similar as in Table S2 but for ^{8}B and ^{9}C.

Nucleus	J^{π}	$E^{\rm exp}(\Gamma^{\rm exp})$	$E^{\rm cal}(\Gamma^{\rm cal})$	Configuration
$^{8}\mathrm{B}_{ps}$	2^{+}	-9.442	-8.970	53% $(0p_{3/2})^{3}_{\rm p}(0p_{3/2})_{\rm n}$ 13% $(0p_{3/2})^{2}_{\rm p}(p^{\rm scatt}_{3/2})_{\rm p}(0p_{3/2})_{\rm n}$ 11% $(0p_{3/2})^{2}_{\rm p}(0p_{1/2})_{\rm p}(0p_{3/2})_{\rm n}$ 8% $(0p_{3/2})^{3}_{\rm p}(0p_{1/2})_{\rm n}$ 3% $(0p_{3/2})^{2}_{\rm p}(0p_{1/2})_{\rm p}(0p_{1/2})_{\rm n}$ 3% $(0p_{3/2})_{\rm p}(0p_{1/2})^{2}_{\rm p}(0p_{3/2})_{\rm n}$ 2% $(0p_{3/2})_{\rm p}(0p_{1/2})_{\rm p}(p^{\rm scatt}_{3/2})_{\rm p}(0p_{3/2})_{\rm n}$ 2% $(0p_{3/2})^{2}_{\rm p}(p^{\rm scatt}_{3/2})_{\rm p}(0p_{1/2})_{\rm n}$
$^{9}\mathrm{C}_{ps}$	$3/2^{-}$	-10.742	-10.515	61% $(0p_{3/2})^{4}_{\rm p}(0p_{3/2})_{\rm n}$ 12% $(0p_{3/2})^{3}_{\rm p}(p^{\rm scatt}_{3/2})_{\rm p}(0p_{3/2})_{\rm n}$ 10% $(0p_{3/2})^{3}_{\rm p}(0p_{1/2})_{\rm p}(0p_{3/2})_{\rm n}$ 8% $(0p_{3/2})^{2}_{\rm p}(0p_{1/2})^{2}_{\rm p}(0p_{3/2})_{\rm n}$ 2% $(0p_{3/2})^{2}_{\rm p}(0p_{1/2})_{\rm p}(p^{\rm scatt}_{3/2})_{p}(0p_{3/2})_{\rm n}$ 2% $(0p_{3/2})^{2}_{\rm p}(p^{\rm scatt}_{3/2})^{2}_{p}(0p_{3/2})_{\rm n}$
	$1/2^{-}$	-8.56(0.1)	-7.583	60% $(0p_{3/2})^{4}_{\rm p}(0p_{3/2})_{\rm n}$ 17% $(0p_{3/2})^{3}_{\rm p}(0p_{1/2})_{\rm p}(0p_{3/2})_{\rm n}$ 9% $(0p_{3/2})^{3}_{\rm p}(p^{\rm scatt}_{3/2})_{\rm p}(0p_{1/2})_{\rm n}$ 4% $(0p_{3/2})^{2}_{\rm p}(0p_{1/2})^{2}_{\rm p}(0p_{1/2})_{\rm n}$ 3% $(0p_{3/2})^{2}_{\rm p}(0p_{1/2})_{\rm p}(p^{\rm scatt}_{3/2})_{\rm p}(0p_{3/2})_{\rm n}$ 2% $(0p_{3/2})^{3}_{\rm p}(p^{\rm scatt}_{3/2})_{\rm p}(0p_{3/2})_{\rm n}$
$^{8}\mathrm{B}_{psd}$	2^{+}	-9.442	-12.817	52% $(0p_{3/2})^{3}_{\rm p}(0p_{3/2})_{\rm n}$ 9% $(0p_{3/2})^{2}_{\rm p}(p^{\rm scatt}_{3/2})_{\rm p}(0p_{3/2})_{\rm n}$ 9% $(0p_{3/2})^{2}_{\rm p}(0p_{1/2})_{\rm p}(0p_{3/2})_{\rm n}$ 4% $(0p_{3/2})^{3}_{\rm p}(0p_{1/2})_{\rm n}$ 3% $(0p_{3/2})^{2}_{\rm p}(0p_{1/2})_{\rm p}(0p_{1/2})_{\rm n}$ 3% $(0p_{3/2})_{\rm p}(0d_{5/2})^{2}_{\rm p}(0d_{5/2})_{\rm n}$ 3% $(0p_{3/2})_{\rm p}(0d_{5/2})^{2}_{\rm p}(0p_{3/2})_{\rm n}$ 3% $(0p_{3/2})_{\rm p}(0p_{1/2})^{2}_{\rm p}(0p_{3/2})_{\rm n}$
$^{9}\mathrm{C}_{psd}$	$3/2^{-}$	-10.742	-9.385	60% $(0p_{3/2})^{4}_{\rm p}(0p_{3/2})_{\rm n}$ 10% $(0p_{3/2})^{3}_{\rm p}(0p_{1/2})_{\rm p}(0p_{3/2})_{\rm n}$ 9% $(0p_{3/2})^{2}_{\rm p}(0p_{3/2})^{2}_{\rm p}(0p_{1/2})_{\rm n}$ 9% $(0p_{3/2})^{3}_{\rm p}(p^{\rm scatt}_{3/2})_{\rm p}(0p_{3/2})_{\rm n}$ 2% $(0p_{3/2})^{3}_{\rm p}(0p_{1/2})_{\rm p}(0p_{1/2})_{\rm n}$ 2% $(0p_{3/2})^{2}_{\rm p}(p^{\rm scatt}_{3/2})^{2}_{\rm p}(0p_{3/2})_{\rm n}$
	$1/2^{-}$	-8.56(0.1)	-5.783	57% $(0p_{3/2})^{4}_{\rm p}(0p_{1/2})_{\rm n}$ 17% $(0p_{3/2})^{3}_{\rm p}(0p_{1/2})_{\rm p}(0p_{3/2})_{\rm n}$ 8% $(0p_{3/2})^{3}_{\rm p}(p^{\rm scatt}_{3/2})_{\rm p}(0p_{1/2})_{\rm n}$ 5% $(0p_{3/2})^{2}_{\rm p}(0p_{1/2})^{2}_{\rm p}(0p_{1/2})_{\rm n}$ 3% $(0p_{3/2})^{2}_{\rm p}(0p_{1/2})_{\rm p}(p^{\rm scatt}_{3/2})(0p_{3/2})_{\rm n}$ 2% $(0p_{3/2})^{2}_{\rm p}(p^{\rm scatt}_{3/2})^{2}_{\rm p}(0p_{1/2})_{\rm n}$ 2% $(0p_{3/2})^{3}_{\rm p}(p^{\rm scatt}_{3/2})_{\rm p}(0p_{3/2})_{\rm n}$

TABLE S4. Similar as in Table S1 but for ^{8,9}Li.

Nucleus	J^π	$E^{\rm exp}(\Gamma^{\rm exp})$	$E^{\rm cal}(\Gamma^{\rm cal})$	Configuration
^{8}Li$_{ps}$	2^+	-12.982	-12.446	57% $(0p_{3/2})^3_n(0p_{3/2})_p$ 12% $(0p_{3/2})^2_n(0p_{1/2})_n(0p_{3/2})_p$ 9% $(0p_{3/2})^2_n(p^{\rm scatt}_{3/2})_n(0p_{3/2})_p$ 8% $(0p_{3/2})^3_n(0p_{1/2})_p$ 3% $(0p_{3/2})^2_n(p_{1/2})_n(0p_{1/2})_p$ 3% $(0p_{3/2})_n(p_{1/2})^2_n(0p_{1/2})_p$ 2% $(0p_{3/2})_n(p_{1/2})_n(p^{\rm scatt}_{3/2})_n(0p_{3/2})_p$
^{9}Li$_{ps}$	$3/2^-$	-17.045	-16.657	65% $(0p_{3/2})^4_{\rm n}(0p_{3/2})_{\rm p}$ 11% $(0p_{3/2})^3_{\rm n}(0p_{1/2})_{\rm n}(0p_{3/2})_{\rm p}$ 9% $(0p_{3/2})^2_{\rm n}(0p_{1/2})^2_{\rm n}(0p_{3/2})_{\rm p}$ 8% $(0p_{3/2})^3_{\rm n}(p^{\rm scatt}_{1/2})_{\rm n}(0p_{3/2})_{\rm p}$
	$1/2^-$	-14.354	-13.561	64% $(0p_{3/2})^4_{\rm n}(0p_{1/2})_{\rm p}$ 18% $(0p_{3/2})^3_{\rm n}(0p_{1/2})_{\rm n}(0p_{3/2})_{\rm p}$ 6% $(0p_{3/2})^3_{\rm n}(p^{\rm scatt}_{3/2})_{\rm n}(0p_{1/2})_{\rm p}$ 4% $(0p_{3/2})^2_{\rm n}(0p_{1/2})^2_{\rm n}(0p_{1/2})_{\rm p}$ 2% $(0p_{3/2})^2_{\rm n}(0p_{1/2})_{\rm n}(p^{\rm scatt}_{3/2})_{\rm n}(0p_{3/2})_{\rm p}$
^{8}Li$_{psd}$	2^+	-12.982	-18.140	56% $(0p_{3/2})^3_n(0p_{3/2})_p$ 9% $(0p_{3/2})^2_n(0p_{1/2})_n(0p_{3/2})_p$ 5% $(0p_{3/2})^3_n(0p_{1/2})_p$ 4% $(0p_{3/2})^2_n(0p_{1/2})_n(0p_{1/2})_p$ 4% $(0p_{3/2})^2_n(p^{\rm scatt}_{3/2})_n(0p_{3/2})_p$ 3% $(0p_{3/2})^2_n(0d_{5/2})_n(0d_{5/2})_p$ 3% $(0p_{3/2})_n(0d_{5/2})^2_n(0p_{3/2})_p$ 3% $(0p_{3/2})_n(0p_{1/2})^2_n(0p_{3/2})_p$ 2% $(0p_{3/2})^2_n(p^{\rm scatt}_{3/2})_n(p^{\rm scatt}_{3/2})_p$
^{9}Li$_{psd}$	$3/2^-$	-17.045	-18.481	64% $(0p_{3/2})^4_{\rm n}(0p_{3/2})_{\rm p}$ 11% $(0p_{3/2})^2_{\rm n}(0p_{1/2})^2_{\rm n}(0p_{3/2})_{\rm p}$ 11% $(0p_{3/2})^3_{\rm n}(0p_{1/2})_{\rm n}(0p_{3/2})_{\rm p}$ 4% $(0p_{3/2})^3_{\rm n}(p^{\rm scatt}_{3/2})_{\rm n}(0p_{3/2})_{\rm p}$ 2% $(0p_{3/2})^3_{\rm n}(0p_{1/2})_{\rm n}(0p_{3/2})_{\rm p}$ 2% $(0p_{3/2})^2_{\rm n}(p^{\rm scatt}_{3/2})^2_{\rm n}(0p_{3/2})_{\rm p}$
	$1/2^-$	-14.354	-14.683	63% $(0p_{3/2})^4_{\rm n}(0p_{1/2})_{\rm p}$ 18% $(0p_{3/2})^3_{\rm n}(0p_{1/2})_{\rm n}(0p_{3/2})_{\rm p}$ 6% $(0p_{3/2})^2_{\rm n}(0p_{1/2})^2_{\rm n}(0p_{1/2})_{\rm p}$ 4% $(0p_{3/2})^3_{\rm n}(p^{\rm scatt}_{3/2})_{\rm n}(0p_{1/2})_{\rm p}$ 2% $(0p_{3/2})^2_{\rm n}(p^{\rm scatt}_{3/2})^2_{\rm n}(0p_{1/2})_{\rm p}$